A guide to lifting aperiodic structures

A guide to lifting aperiodic structures

Michael Baake[1], David Écija[2] and Uwe Grimm[3]

The embedding of a given point set with non-crystallographic symmetry into higher-dimensional space is reviewed, with special emphasis on the Minkowski embedding known from number theory. This is a natural choice that does not require an a priori construction of a lattice in relation to a given symmetry group. Instead, some elementary properties of the point set in physical space are used, and explicit methods are described. This approach works particularly well for the standard symmetries encountered in the practical study of quasicrystalline phases. We also demonstrate this with a recent experimental example, taken from a sample with square-triangle tiling structure and (approximate) twelvefold symmetry.

1 Introduction

Ever since the discovery of quasicrystals [12], one standard approach to the investigation of direct images of aperiodic structures consists of 'lifting' a set of positions in two- or three-dimensional space into a higher-dimensional space, sometimes referred to as 'superspace'. For instance, this could be a set of positions obtained from electron miscroscopy of a thin slice of a quasicrystal, or from an STM image of a surface. The lift then provides important information about the structure of the quasicrystal in terms of a cut and project description. From a mathematical point of view, such data sets are represented as point sets in space (for instance as sets of atomic or cluster positions), and we are interested in lifting such a point set into a higher-dimensional space in a suitable way that reveals more of the underlying structure.

This approach is particularly useful if the lifted positions come to lie on a lattice in the higher-dimensional space, so the lift produces an embedding of the point set into a lattice. Here, a *lattice* $\varGamma$ in d-dimensional real space $\mathbb{R}^d$ is defined as the integer span of a set of d linearly independent vectors e_i, $1 \le i \le d$, so that

$$\varGamma = \Big\{ \sum_{i=1}^{d} n_i e_i \;\big|\; \text{all } n_i \in \mathbb{Z} \Big\} \quad \text{and}$$

$$\mathbb{R}^d = \Big\{ \sum_{i=1}^{d} x_i e_i \;\big|\; \text{all } x_i \in \mathbb{R} \Big\}.$$

In the literature, one will often find such lifts described for situations where the higher-dimensional lattice is known in advance. This may give the impression that, in order to apply this approach to an observed set of positions, one has to choose a lattice at the start, which will generally not be unique. However, it may not be obvious what lattice to choose, which asks for some canonical choice.

In fact, it is possible to employ an *intrinsic* approach where the lattice is constructed from the observed set of positions directly, for instance by recovering the 'missing part' of the higher-dimensional coordinates. That this is indeed possible for 'quasicrystalline' structures follows from a non-trivial theorem in [2]. It is the goal of this paper to demonstrate that the underlying construction, in many relevant situations, is feasible and actually surprisingly simple.

This approach is not new – in fact, it is pretty much the standard way it is done in parts of mathematics, in particular in number theory. Since the quasicrystal structures that are observed do have a close connection with these number-theoretic structures, it seems worth-while to explain the connection and the resulting methods in the context of quasicrystalline point sets. In this sense, the present article can be seen as a pedagogic attempt to simplify the handling of point sets with certain practically relevant symmetries [13]. As such, it is a continuation of core material from the recent monograph [1], which also serves as our main reference for further examples and various mathematical details.

Below, we describe how the lifting can be done, both in theory and in practice. We start with simple model systems in one dimension, and then discuss planar examples with eight- and twelvefold symmetry. Finally, we apply our method to an experimental dataset. Let us mention that the same approach also works for structures with icosahedral symmetry, as briefly explained in [1, Sec. 3.4.3]. We will not discuss this case below and refer the interested reader to this source and to the references given therein.

[1] *Fakultät für Mathematik, Universität Bielefeld, Postf. 100131, 33501 Bielefeld, Germany. E-mail: mbaake@math.uni-bielefeld.de*

[2] *IMDEA Nanociencia, C/Faraday, 9, Campus Universitario de Cantoblanco, 28049 Madrid, Spain. E-mail: david.ecija@imdea.org*

[3] *School of Mathematics and Statistics, The Open University, Walton Hall, Milton Keynes MK7 6AA, United Kingdom. Email: uwe.grimm@open.ac.uk*

2 One-dimensional examples

Let us start with a classic example which is based on the symbolic *substitution* rule $a \mapsto aba$, $b \mapsto a$ for the binary alphabet $\{a, b\}$. Considering a and b as two intervals of lengths $\lambda = 1 + \sqrt{2}$ and 1, the corresponding geometric *inflation* rule is

which maps an interval of type a to three consecutive intervals aba, and the interval b to a; see [1, Def. 4.8] for a more detailed description of substitution versus inflation rules. We start from a pair of intervals of type a (which, on the symbolic level, is a legal word of length two because it appears in the second iterate of the letter a) with the origin as its common vertex point. A repeated application of the inflation rule produces a one-dimensional tiling of the real line by intervals of type a and b, according to the symbolic sequence

$$a|a \mapsto aba|aba \mapsto abaaaba|abaaaba \mapsto$$
$$abaaabaabaabaaaba|abaaabaabaabaaaba \mapsto \ldots \longrightarrow w$$

which converges to a sequence w that is fixed by the substitution rule (and the corresponding tiling is fixed by the inflation rule). Here, the vertical line denotes the position of the origin, and the sequence (as well as the corresponding geometric tiling) is clearly symmetric under reflection in the origin. The sequence w is often referred to as the *silver-mean sequence* due to the continued fraction expansion $[2; 2, 2, 2, 2, \ldots]$ of $\lambda = 1 + \sqrt{2}$.

Now, collating the left endpoints of each interval of type a and the left endpoints of intervals of type b produces two point sets $\varLambda_a$ and $\varLambda_b$. Their union $\varLambda = \varLambda_a \cup \varLambda_b \subset \mathbb{R}$ is called the *silver mean point set*. By construction, it contains the origin. Because the two interval lengths are λ and 1, the distance between neighbouring points is either λ or 1, and all points must be positioned at integer linear combinations of these two numbers. Hence, $\varLambda \subset L$ where

$$L = \mathbb{Z}[\sqrt{2}] = \{m + n\sqrt{2} \mid m, n \in \mathbb{Z}\}.$$

The set L is a dense point set in $\mathbb{R}$, and it is the ring of integers in the quadratic number field $\mathbb{Q}(\sqrt{2})$, which is the smallest field extension of the rational numbers that contains $\sqrt{2}$. This field has a unique non-trivial automorphism which is algebraic conjugation, defined by $\sqrt{2} \mapsto -\sqrt{2}$. For a number $x = m + n\sqrt{2} \in L$, we denote its algebraic conjugate by $x^\star = m - n\sqrt{2}$.

Using algebraic conjugation, a natural embedding of L in $\mathbb{R}^2$ is given by

$$\mathcal{L} = \big\{(x, x^\star) \mid x \in L\big\} \subset \mathbb{R}^2,$$

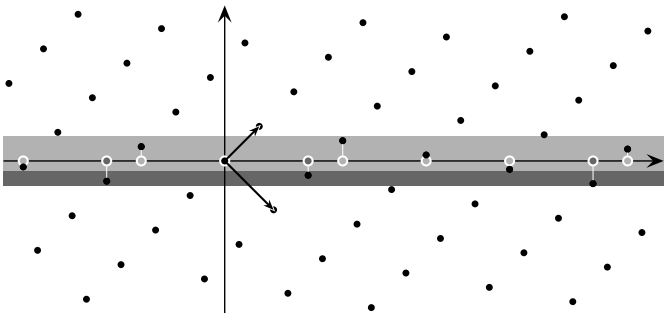

Figure 1: The rectangular lattice $\mathcal{L}$ (black dots) is generated by the vectors $(1, 1)$ and $\sqrt{2}(1, -1)$. Points in $\varLambda_a$ (light grey) lift into lattice points within the upper (light grey) strip, points in $\varLambda_b$ (dark grey) lift into lattice points within the lower (dark grey) strip. All lattice points within these strips are obtained in this way.

which is called the *Minkowski embedding* of L; compare [1, Ch. 3.4]. What does $\mathcal{L}$ look like? Its elements (written as row vectors) are of the form

$$(m + n\sqrt{2}, m - n\sqrt{2}) = m\,(1, 1) + n\,(\sqrt{2}, -\sqrt{2})$$

with $m, n \in \mathbb{Z}$, and the representation on the right-hand side shows that $\mathcal{L}$ is a lattice which is spanned by the two vectors $(1, 1)$ and $\sqrt{2}\,(1, -1)$. These two vectors are clearly orthogonal, so that $\mathcal{L}$ is a rectangular lattice in the plane; see Figure 1 for an illustration.

We thus know that the lift $x \mapsto (x, x^\star)$ maps points in our silver mean point set $\varLambda$ into $\mathcal{L}$, so

$$\big\{(x, x^\star) \mid x \in \varLambda\big\} \subset \mathcal{L}.$$

In our example, this turns out to be a very special subset indeed, as can be seen from Figure 1. Explicitly, all left endpoints of intervals of type a occur at positions $x \in L$ with $-\frac{2-\sqrt{2}}{2} \le x^\star \le \frac{\sqrt{2}}{2}$, while all left endpoints of intervals of type b are located at positions $x \in L$ with $-\frac{\sqrt{2}}{2} \le x^\star \le -\frac{2-\sqrt{2}}{2}$. Note that there are no points in L for which $x^\star$ falls onto the boundaries of these intervals (because the boundary points are not in L due to the factor $\frac{1}{2}$), so there is no ambiguity here. The silver mean point set can now be characterised as the *model set* (or cut-and-project set)

$$\varLambda = \{x \in L \mid x^\star \in W\}$$

with the window W being the interval $W = [-\frac{\sqrt{2}}{2}, \frac{\sqrt{2}}{2}]$ which swipes out the grey strips in Figure 1. For the proof of these statements, we refer to [1, Ch. 7.1].

At this point, we can lift any subset $S \subset L$, which is a set in *direct* (or physical) space into *internal* space as

$$S^\star = \{x^\star \mid x \in S\}.$$

If we do this for the set $\varLambda$, we find that $\varLambda^\star$ is a dense subset of the window. Moreover, if we do this for the finite subsets of the form $\varLambda_r := \varLambda \cap [-r, r]$, the sets $\varLambda_r^\star$ are finite point sets inside the window W that fill it out more and more with increasing r. In fact, this is done in a uniform way, which is an important feature known as *uniform distribution*; see [1, Prop. 7.3] for more.

Let us note two important things at this point. First, the lift is done by extracting the missing internal space part $x^\star$ from the known coordinate x in direct space, so that the lift is given by $x \mapsto (x, x^\star)$. Second, the lattice and the required algebraic information is entirely obtained from the set $\varLambda$, respectively from the set L that emerged from $\varLambda$ via integer linear combinations. The correct identification of L from $\varLambda$ can be a little more delicate than in our example at hand, as is well-known from examples such as the Penrose tiling vertices; compare [1, Ex. 7.11]. Since we will not meet such cases below, we suppress the necessary identification of the *limit translation module* and refer the reader to [1, Sec. 5.1.2] for further details.

Note that, in the construction above, we did not start from a given lattice, but constructed $\mathcal{L}$ as the Minkowski embedding of the underlying arithmetic structure of the point set. In this sense, this is a natural embedding, but we are still free to modify the choice of lattice by changing the relative scale between the direct and the internal space. Concretely, one could also use

$$\mathcal{L}_\alpha \,:=\, \bigl\{(x, \alpha x^\star) \mid x \in L\bigr\}$$

for any positive α, so that our previous choice satisfies $\mathcal{L} = \mathcal{L}_1$. In principle, even negative α can be used, but since this only results in a reflection in the x-axis, we restrict our attention to $\alpha > 0$. The spanning vectors of $\mathcal{L}_\alpha$ can now be chosen as $b_1 = (1, \alpha)$ and $b_2 = (\sqrt{2}, -\alpha\sqrt{2})$. For special choices of α, the lattice $\mathcal{L}_\alpha$ will actually be a (scaled) square lattice. For instance, this happens for $\alpha = \lambda$ (where $\mathcal{L}_\lambda$ is then spanned by $b_1 = (1, \lambda)$ and $b_2' = b_1 + b_2 = (\lambda, -1)$), but also for $\alpha = 1/\lambda = \lambda - 2$ (where $\mathcal{L}_{1/\lambda}$ is spanned by $b_1 = (1, \lambda - 2)$ and $b_2' = b_2 - b_1 = (\lambda - 2, -1)$).

Although any of these choices seems 'nice' in the sense that the square lattice has a higher symmetry than the original Minkowski embedding, it should be emphasised that this symmetry is perhaps appealing, but of no relevance to the problem at hand. This is so because the relative scale between direct and internal space is just a number, without *any* physical meaning.

A completely analogous situation emerges for the well-known Fibonacci inflation rule

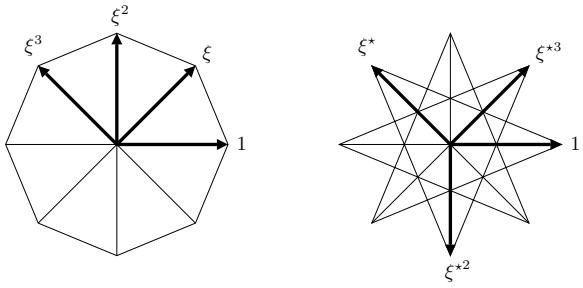

Figure 2: The regular 8-star in direct space (left panel) with $\xi = \xi_8 = \mathrm{e}^{2\pi\mathrm{i}/8}$ and its $\star$-image in internal space (right panel). Here, $\xi^\star = \xi^3$ and $1^\star = 1$, as well as $(\xi^n)^\star = (\xi^\star)^n$.

with intervals of length τ and 1 as prototiles, where τ is the golden ratio. Here, the dense point set spanned by the positions of the left endpoints is $L = \mathbb{Z}[\tau]$, the ring of integers in the quadratic field $\mathbb{Q}(\sqrt{5})$, and the non-trivial field automorphism is defined by $\sqrt{5} \mapsto -\sqrt{5}$, which means $\tau \mapsto \tau^\star = \frac{-1}{\tau} = 1 - \tau$ and hence

$$m + n\tau \;\longmapsto\; (m + n\tau)^\star = \, m + n - n\tau.$$

Here, the Minkowski embedding is spanned by $(1, 1)$ and $(\tau, 1 - \tau)$, which is not even a rectangular lattice; see [1, Fig. 3.3] for an illustration. As before, by scaling internal space relative to direct space, one can turn the embedding lattice into a square lattice, as discussed in [1, Rem. 3.4]. Still, the same comment from above applies, meaning that such a rescaling of internal space bears no physical relevance.

3 Eightfold symmetric tilings

The basic object for eightfold symmetry is the regular 8-star, as shown in the left panel of Figure 2, where it is natural to use vectors of length 1. Identifying $\mathbb{R}^2$ with $\mathbb{C}$ as usual, the 8-star is nothing but the star of all 8th roots of unity, that is the eight solutions of the equation $z^8 - 1 = 0$. Let ξ_8 be a *primitive* solution (meaning that $\xi_8^n = 1$ only holds for integers that are divisible by 8), for instance $\xi_8 = \mathrm{e}^{2\pi\mathrm{i}/8}$ to be explicit (the other primitive solutions being ξ_8^3, ξ_8^5 and ξ_8^7).

The analogue of the dense point set L from the previous section is $L_8 = \mathbb{Z}[\xi_8]$, the ring of integers in the cyclotomic field $\mathbb{Q}[\xi_8]$; see [1, Sec. 2.5.2] for an introduction in our context. Any element of L_8 is an integer linear combination of $1, \xi_8, \xi_8^2, \ldots, \xi_8^7$, but it turns out that the first four of them suffice, so

$$L_8 \,=\, \{m_0 1 + m_1\xi_8 + m_2\xi_8^2 + m_3\xi_8^3 \mid \text{all } m_i \in \mathbb{Z}\}.$$

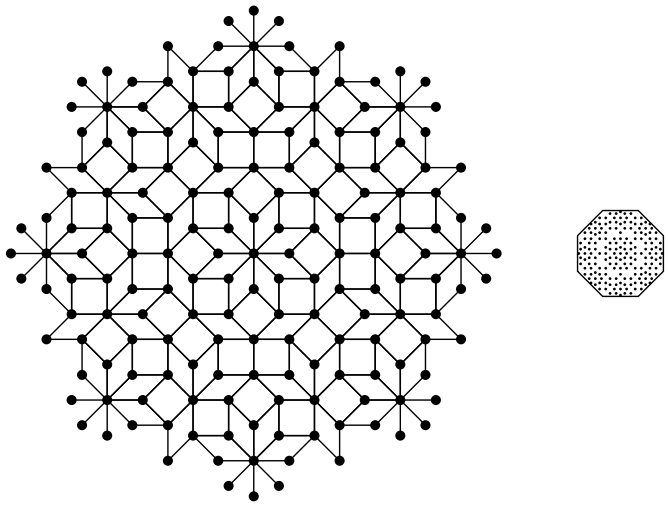

Figure 3: An 8-fold symmetric patch of the Ammann–Beenker tiling (left panel) and the lift of its vertex point set to internal space via the $\star$-map for the $\mathbb{Z}$-module L_8 (right panel); see text for details.

Alternatively, one also has that

$$L_8 \;=\; \bigl\{\alpha_0 1 + \alpha_1 \xi_8 \mid \text{all } \alpha_i \in \mathbb{Z}[\sqrt{2}\,]\bigr\},$$

which means that L_8 is a $\mathbb{Z}$-module of rank 4 and, at the same time, a $\mathbb{Z}[\sqrt{2}\,]$-module of rank 2. The latter property lines up with L_8 being a dense subset of $\mathbb{C} \simeq \mathbb{R}^2$, while the former tells us that a lift to a lattice will need $\mathbb{R}^4$. Let us thus turn to the construction of the lattice.

The crucial point is the selection of the $\star$-map. In our context, it has to be one of the field automorphisms of $\mathbb{Q}(\xi_8)$; see [1, Secs. 2.5.2 and 3.4.2] for details. Clearly, it can neither be complex conjugation nor the trivial one, which leaves us with the choices $\xi_8 \mapsto \xi_8^3$ or $\xi_8 \mapsto \xi_8^5$, together with the unique extension to a field automorphism. Either choice is fine. Let us use the first one for convenience, so that $(\xi_8^n)^\star = (\xi_8^\star)^n = \xi_8^{3n}$ for $n \in \mathbb{Z}$. The effect on the regular 8-star is shown in the right panel of Figure 2. Now, the Minkowski embedding gives the lattice

$$\mathcal{L}_8 \;=\; \bigl\{(x, x^\star) \mid x \in L_8\bigr\} \;\subset\; \mathbb{R}^4.$$

One can show that $\mathcal{L}_8$ is a scaled (by a factor of $\sqrt{2}\,$) and rotated version of the integer lattice $\mathbb{Z}^4$; see [1, Ex. 3.6].

As an example, let us consider the central patch of the 8-fold symmetric Ammann–Beenker tiling shown in the left panel of Figure 3. We assume this patch to be generated by the inflation rule of [1, Sec. 6.1], applied to prototiles of unit edge length. If we give the central vertex the coordinate $0 \in L_8$, any other vertex of the patch is an element of L_8 as well, because every edge has unit length and corresponds to one of the directions of the regular 8-star. Therefore, each vertex can uniquely be indexed by

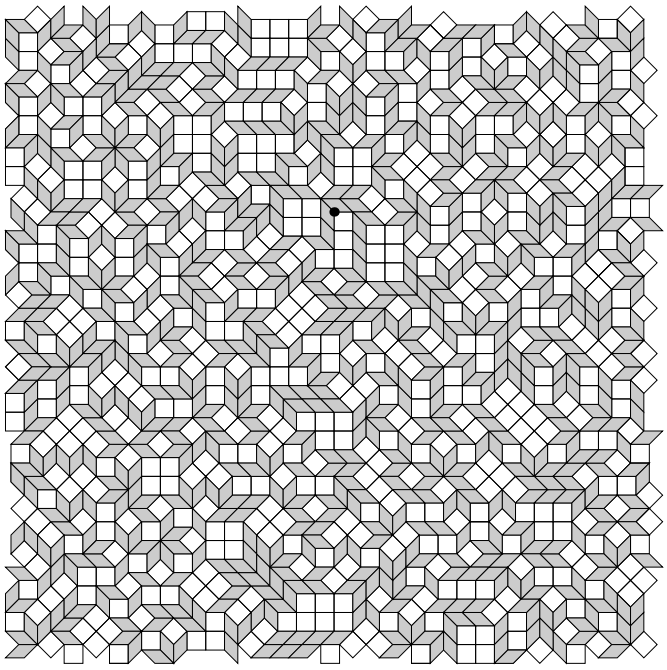

Figure 4: A typical patch of an octagonal random tiling with statistical 8-fold symmetry. The marked vertex point has been used as the origin.

a 4-tuple of integers, (m_0, m_1, m_2, m_3), which represents the point

$$x \;=\; m_0 1 + m_1 \xi_8 + m_2 \xi_8^2 + m_3 \xi_8^3$$

in direct space. Concretely, one finds these 4-tuples by starting from the origin and going along the tile edges to the other vertex points, where each edge with its direction corresponds positively or negatively to one of the first four vectors of the regular 8-star; compare the left panel of Figure 2. Since the sum of all vectors of the 8-star vanishes, the result does not depend on the path that was chosen.

Given any point (m_0, m_1, m_2, m_3) in L_8, its $\star$-image is the point

$$x^\star \;=\; m_0 1 + m_1 \xi_8^3 - m_2 \xi_8^2 + m_3 \xi_8$$

in internal space. In terms of the original basis, the $\star$-map amounts to the mapping

$$(m_0, m_1, m_2, m_3) \;\mapsto\; (m_0, m_3, -m_2, m_1)$$

which really is quite simple! Its action on the vertex points of our Ammann–Beenker patch is shown in the right panel of Figure 3. The point cloud is the lift of the patch and lies within a regular octagon of unit edge length, in line with the known fact that the vertex set of the Ammann–Beenker tiling is a cut and project set (or model set) for the lattice $\mathcal{L}_8$ with the octagon as its window (or acceptance

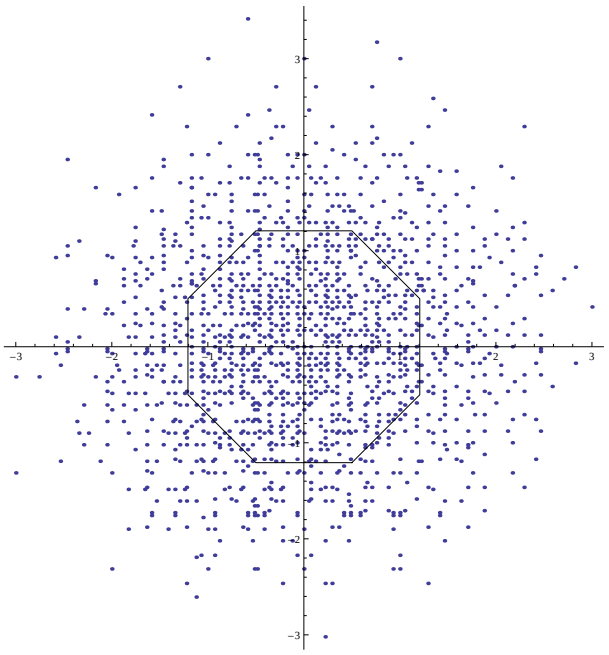

Figure 5: Lift of the vertex points of the octagonal random tiling patch of Figure 4 to internal space via the $\star$-map. The octagonal window of the perfect Ammann–Beenker tiling is shown in the correct relative size.

domain); see [1, Sec. 7.3] for a detailed exposition. An important feature of a regular model set such as this one is the fact that the lifted points, in a natural order according to their distance from the centre in direct space, are uniformly distributed in the window in internal space. This is a strong homogeneity property of the system, which facilitates the calculation of statistical properties as well as a closed formula for the kinematic diffraction of the point set.

Let us contrast this perfectly ordered structure with its random tiling counterpart of Figure 4, which was obtained via repeated simpleton flips from a perfect patch as described in [1, Sec. 11.6.2] and references therein. Still, choosing any vertex point as the origin, all vertex points of the patch are elements of L_8, and hence can be lifted via the same $\star$-map and the method described above. The result is shown in Figure 5, with the chosen origin marked (a different choice would just result in a shift of the lifted point set). It is clearly visible that the set of lifted positions extends beyond the window of the perfect tiling, in agreement with the expectation for the statistics of random tilings [6].

The very same method, with minor modifications, works for any rhombus tiling with edges along the directions of a regular n-star. In fact, it also works if we have a set of prototiles with edges of the same length along such a set of directions. In general, the dimension of the internal space becomes larger; see [1, Sec. 7.3] for details. Here, we restrict our attention to the practically most important cases where internal space has the same dimension as direct space. In view of dodecagonal quasicrystals [8, 3] and various recent developments, the possibly most relevant example is that of 12-fold symmetry, with square-triangle tilings featuring prominently; see [15, 9, 10, 4] and references therein.

4 Square-triangle tilings

The analogue of Figure 2 for 12-fold symmetry is given by the regular 12-star of Figure 6 (left panel) and its $\star$-image (right panel). The integer span of the regular 12-star is

$$L_{12} \,=\, \{m_0 1 + m_1\xi_{12} + m_2\xi_{12}^2 + m_3\xi_{12}^3 \mid \text{all } m_i \in \mathbb{Z}\}\,,$$

which is once again a $\mathbb{Z}$-module of rank 4. In particular, one has $\xi_{12}^4 = \xi_{12}^2 - 1$ and $\xi_{12}^5 = \xi_{12}^3 - \xi_{12}$, while the remaining powers of ξ_{12} are obtained via multiplication by -1 from the powers so far.

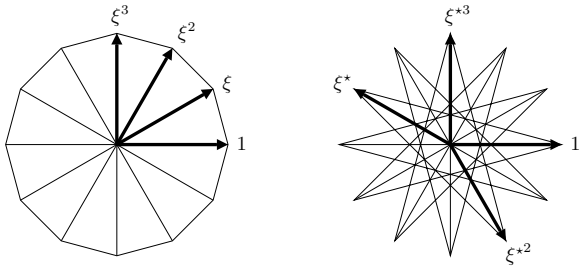

Figure 6: The regular 12-star in direct space (left panel) with $\xi = \xi_{12} = \mathrm{e}^{2\pi\mathrm{i}/12}$ and its $\star$-image in internal space (right panel), where $\xi^\star = \xi^5$. Note that $\xi^3 = (\xi^\star)^3 = \mathrm{i}$.

The module L_{12} is also a $\mathbb{Z}[\sqrt{3}\,]$-module of rank 2, meaning that

$$L_{12} \,=\, \big\{\alpha_0 1 + \alpha_1\xi_{12} \mid \text{all } \alpha_i \in \mathbb{Z}[\sqrt{3}\,]\big\},$$

see [1, Sec. 2.5.2] for details. As in our previous example, the $\star$-map is one of the suitable field automorphisms of the cyclotomic field $\mathbb{Q}(\xi_{12})$. Here, one has the choice between $\xi_{12} \mapsto \xi_{12}^5$ and $\xi_{12} \mapsto \xi_{12}^7$, where we have selected the former. The action on the 12-star is shown in Figure 6.

In this case, the $\star$-image of a point (m_0, m_1, m_2, m_3) in L_{12} is given by

$$x^\star \,=\, (m_0 + m_2)1 - m_1\xi_{12} - m_2\xi_{12}^2 + (m_1 + m_3)\xi_{12}^3$$

in internal space. Hence, the $\star$-map acts on the 4-tuples of integer coordinates as

$$(m_0, m_1, m_2, m_3) \,\mapsto\, (m_0 + m_2, -m_1, -m_2, m_1 + m_3)\,.$$

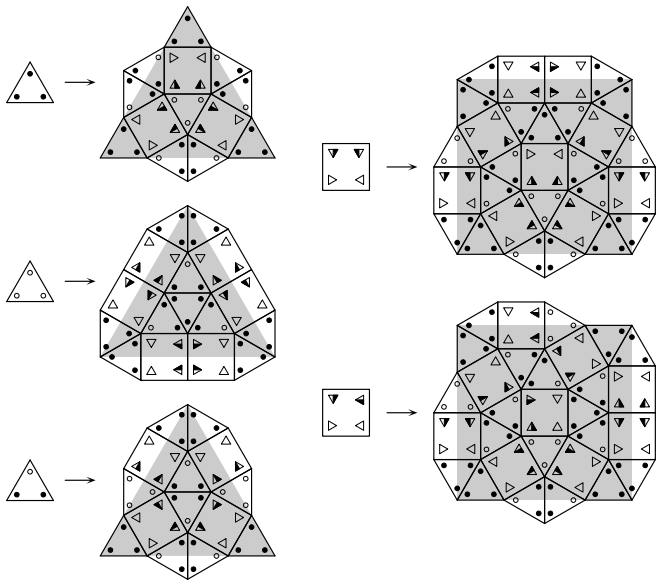

Figure 7: Schlottmann's pseudo inflation rule for a square-triangle tiling formulated via five decorated prototiles (up to similarity).

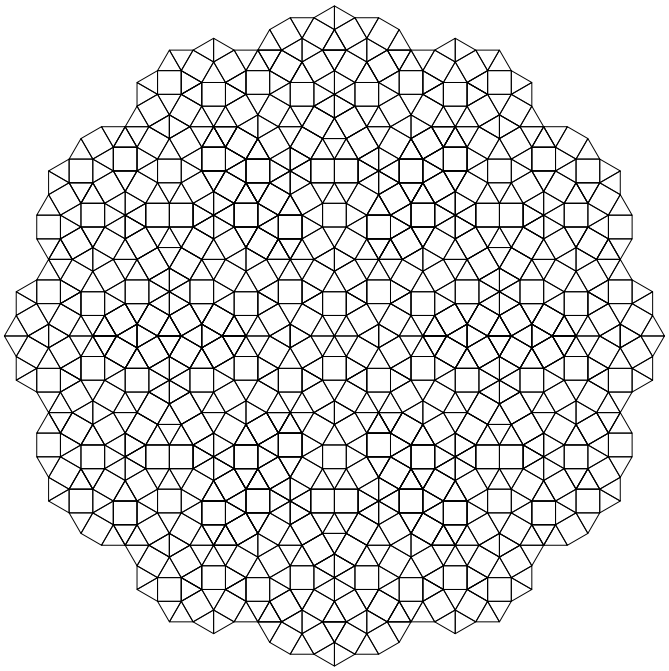

Figure 8: A patch of the square-triangle tiling obtained via the pseudo inflation rule of Figure 7. Note that the decorations are required to construct the patch, but have been omitted in this figure.

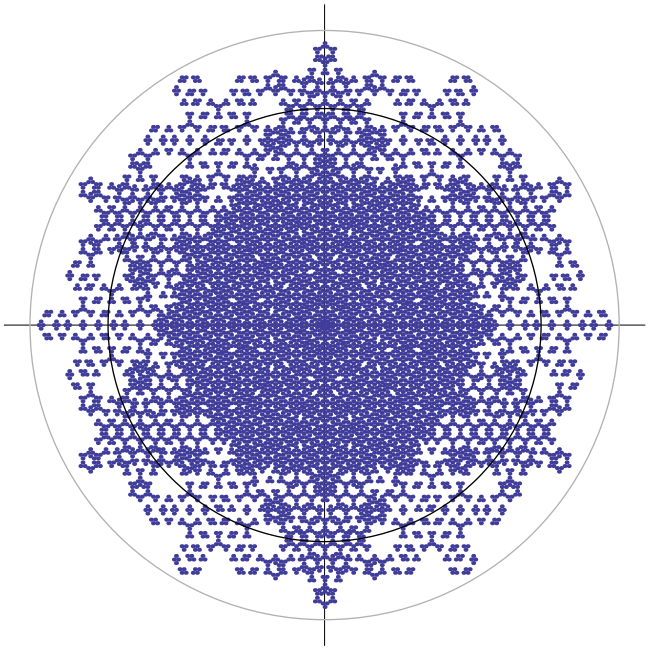

Figure 9: Lift of the vertex points of the next inflation step of the square-triangle patch of Figure 8 to internal space via the $\star$-map. The black circle indicates the size of a circular window for a cut and project set of the same density. Note that the exact sixfold symmetry is a consequence of the corresponding symmetry of the underlying patch, while the 12-fold symmetry of the fractally bounded window will only emerge in the infinite size limit. The grey circle indicates the circumcircle of the (fractally bounded) window.

We are now prepared to lift arbitrary subsets of L_{12} to internal space. Let us note that there is a canonical Minkowski embedding again, leading to the lattice $\mathcal{L}_{12} = \{(x, x^\star) \mid x \in L_{12}\} \subset \mathbb{R}^4$. Of course, one could also use $\{(x, \alpha x^\star) \mid x \in L_{12}\}$ with $\alpha > 0$, which gives us the freedom to select a 'nice' lattice in 4-space; see [1, Ex. 3.6 and Rem. 3.5] for details. However, as explained in Section 2 above, the parameter α has no physical relevance whatsoever and is not needed to describe the lift or the structure in direct space. Therefore, we prefer to dispense with it altogether for our discussion.

This setting can now be applied to 12-fold rhombus tilings, but also to examples such as Gähler's shield tiling, see [5] or [1, Sec. 6.3.2], or to the large family of square-triangle tilings. Let us consider the latter case, and apply the setting to the 12-fold symmetric square-triangle tiling of the plane that is obtained by Schlottmann's pseudo inflation rule of Figure 7; see [1, Sec. 6.3.1] and references therein for background. A patch of the (undecorated) tiling is shown in Figure 8. It is known that the vertex

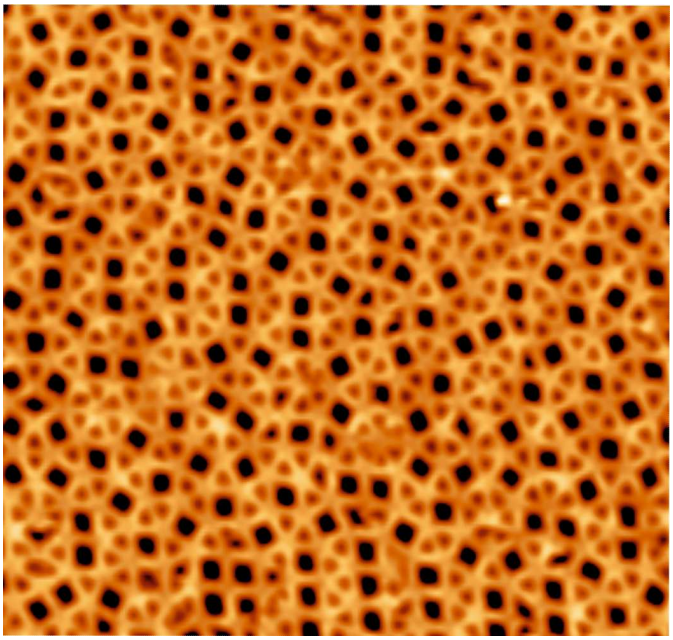

Figure 10: STM image of a metal-organic coordination network [14].

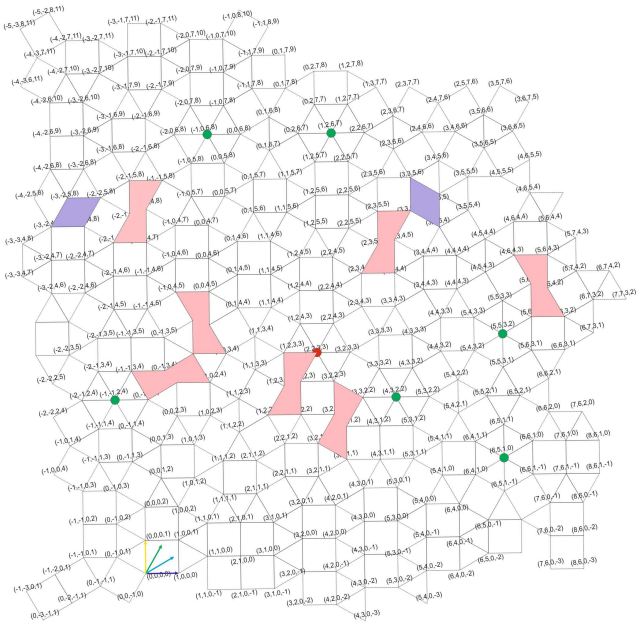

Figure 11: Square-triangle tiling (with defects) obtained by explicit, slightly idealised coordinatisation from the experimental STM image of Figure 10. Note that the choice of origin is arbitrary. See text for further details.

points of this tiling form a cut and project set (or model set), where the window is a 12-fold symmetric region in the plane with fractal boundary; see [1, Fig. 7.10 and Rem. 7.9]. From the inflation rule, one can calculate that the vertex point set has density $(3+2\sqrt{3})/6 \approx 1.077$. Since the lattice $\mathcal{L}_{12}$ has density $\frac{1}{3}$ in 4-space, the area of the window must be $(3+2\sqrt{3})/2$. This implies that a model set with a circular window of radius $\sqrt{(3+2\sqrt{3})/2\pi} \approx 1.014$ would be a point set of the same density (which differs in many positions though).

The result of the lift to internal space via the $\star$-map is shown in Figure 9. Here, we have started from the patch that emerges from Figure 8 by one additional inflation step, which has 8623 vertices. For comparison, the circular window mentioned above is indicated in the figure. While some lifted points fall outside this circle, they remain within the window of the square-triangle tiling which is the compact set of [1, Fig. 7.10].

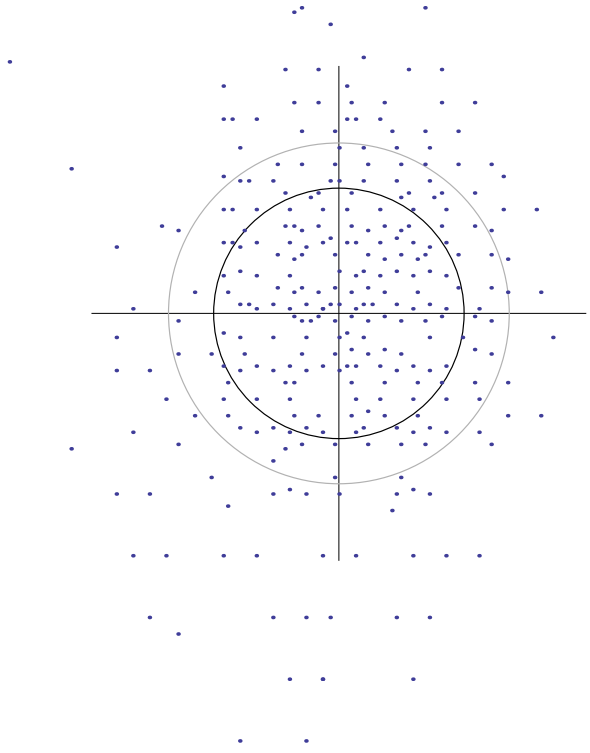

Figure 12: Lift of the vertex points of the experimental tiling of Figure 11 to internal space via the $\star$-map. The figure is centred in the barycentre of the point cloud. The two circles then exactly correspond to those of Figure 9; see text for further details.

5 Sample application

Let us finally apply the method to Figure 10, which shows an experimental STM image [14]. It was obtained by STM analysis of a metallo-supramolecular network, which is based on Europium-ligand coordination motifs. The molecules appear as rod-like protrusions in the STM data, whereas Eu atoms reside at the intersection points. We identify distinct coordination nodes which are intercon-

nected by certain molecular linkers and span an intricate, fully reticulated metallo-supramolecular network. The individual Eu centres are surrounded by four, five or six molecules. Moreover, the Eu vertices and linker backbones are distributed in such a fashion that the design can be interpreted as a surface tessellation based on a square-triangle tiling with defects; see Figure 11 for the result with explicit 4D integer coordinates.

Locally sixfold configurations have been marked by a thicker vertex point, and two different types of defects have been highlighted. The lozenge-shaped defects simply indicate a missing link in the structure, but do not create any conflict with a square triangle tiling, because the lozenge consists of two regular triangles. In contrast, the 'diabolo'-shaped regions are remaining areas that cannot be tiled by squares and triangles, and thus indicate a more profound structural imperfection. A similar comment applies to the 'shield'-shaped region in the upper right part of Figure 11; see [14] (and its supplement) for a more detailed discussion. Since all coordinatised vertices are elements of our module L_{12}, the lifting procedure is not affected by the existence of such regions.

Figure 12 shows the corresponding lift to internal space by our previously described method. The orientations correspond to the right panel of Figure 6. The two circles in Figure 12 exactly correspond to those of Figure 9. Here, the distribution of lifted points clusters around the barycentre, but is both less regular and more spread out than the points from a perfect cut and project set. In particular, one sees a preferred direction. Note that the spreading of the point cloud is an indication of a global structural disorder, and not just a result of the isolated defects. For a related discussion in the context of decagonal quasicrystals, we refer to [7]. Further interpretations and details can be found in [14].

Acknowledgements

It is our pleasure to thank Johannes Roth for useful hints. We are grateful to Johannes V. Barth, Nian Lin and José I. Urgel for providing the experimental image from [14]. D.É. would like to thank the TU Munich physics department for hospitality, where part of the research was done. This work was supported by the German Research Foundation (DFG), within the CRC 701, as well as by the Spanish Ministerio de Economía y Competitividad (project FIS 2015-67287-P).

References

[1] M. Baake and U. Grimm, *Aperiodic Order. Vol. 1: A Mathematical Invitation* (Cambridge University Press, Cambridge, 2013).

[2] M. Baake and R.V. Moody, *Weighted Dirac combs with pure point diffraction*, J. Reine und Angew. Math. (Crelle) **573** (2004) 61–94; math.MG/0203030.

[3] M. Conrad, F. Krumeich and B. Harbrecht, *A dodecagonal quasicrystalline chalcogenide*, Angew. Chem. Int. Ed. **37** (1998) 1383–1386.

[4] T. Dotera, T. Oshiro and P. Ziherl, *Mosaic two-lengthscale quasicrystals*, Nature **506** (2014) 208–211.

[5] F. Gähler, *Quasicrystal Structures from the Crystallographic Viewpoint*, PhD thesis no. 8414 (ETH Zürich, 1988).

[6] C.L. Henley, *Random tiling models*, in: *Quasicrystals: The State of the Art*, 2nd ed., eds. D.P. DiVincenzo and P.J. Steinhardt (World Scientific, Singapore, 1999) pp. 459–560.

[7] T. Ishimasa, *Dodecagonal quasicrystals still in progress*, Isr. J. Chem. **51** (2011) 1216–1225.

[8] T. Ishimasa, H.-U. Nissen and Y. Fukano, *New ordered state between crystalline and amorphous in Ni-Cr particles*, Phys. Rev. Lett. **55** (1985) 511–513.

[9] R. Lifshitz and H. Diamant, *Soft quasicrystals — Why are they stable?* Phil. Mag. **87** (2007) 3021–3030; `arXiv:cond-mat/0611115`.

[10] J. Mikhael, J. Roth, L. Helden and C. Bechinger, *Archimedean-like tiling on decagonal quasicrystalline surfaces*, Nature **454** (2008) 501–504.

[11] R.V. Moody, *Model sets: A survey*, in: *From Quasicrystals to More Complex Systems*, eds. F. Axel, F. Dénoyer and J.P. Gazeau (EDP Sciences, Les Ulis, and Springer, Berlin, 2000) pp. 145–166; `arXiv:math.MG/0002020`.

[12] D. Shechtman, I. Blech, D. Gratias and J.W. Cahn, *Metallic phase with long-range orientational order and no translational symmetry*, Phys. Rev. Lett. **53** (1984) 1951–1953.

[13] W. Steurer, *Twenty years of structure research on quasicrystals. Part I. Pentagonal, octagonal, decagonal and dodecagonal quasicrystals*, Z. Kristallogr. **219** (2004) 391–446.

[14] J.I. Urgel, D. Écija, G. Lyu, R. Zhang, C.-A. Palma, W. Auwärter, N. Lin and J.V. Barth, *Quasicrystallinity expressed in two-dimensional coordination networks*, Nature Chem. (2016), published online at doi:10.1038/nchem.2507.

[15] X. Zeng, G. Ungar, Y. Liu, V. Percec, A.E. Dulcey and J.K. Hobbs, *Supramolecular dendritic liquid quasicrystals*, Nature **428** (2004) 157–160.